NONLINEAR STABILITY ANALYSIS OF WHIRL FLUTTER IN A TILTROTOR ROTOR-NACELLE SYSTEM

Mr Christopher Mair[1], Dr Djamel Rezgui[2] and Dr Branislav Titurus[3]
Department of Aerospace Engineering, University of Bristol, Queens Building, Bristol, UK

Abstract

Whirl flutter is an aeroelastic instability that affects propellers/rotors and the vicinity in which they are mounted. Whirl flutter analysis in tiltrotors gets progressively more complicated with the addition of nonlinear effects. This paper investigates the impact of nonlinear pylon stiffness on the whirl flutter stability of a basic rotor-nacelle model, compared to a baseline linear stiffness version. The nonlinearity investigated in this paper is cubic stiffening of both softening and hardening profiles. The investigation is conducted through a combination of simulations, eigenvalue and bifurcation analyses, in order to fully capture the effects of spring nonlinearity on the dynamic behaviour of the rotor-nacelle system. The analysis provides a more complete stability envelope, demonstrating the complex behaviour of the rotor-nacelle system in the presence of cubic stiffening. The results illustrate the coexistence of stable and unstable limit cycles and equilibria for a range of parameter values. The results also demonstrate the importance of nonlinear whirl flutter models and analysis methods. Of particular interest are cases where the dynamics of the nacelle are unstable despite linear analysis predicting stable behaviour.

1. INTRODUCTION

Tiltrotors such as the ERICA tiltrotor concept shown in Figure 1 are a technology area of growing importance due to their potential solution of the airport congestion problem worldwide. This requires tiltrotors with the passenger capacity of a regional jet to be developed, which is substantially larger than any existing models. The aero-elastic instability known as whirl flutter is an important consideration in the design of this type of aircraft, particularly in the presence of nonlinearity and uncertainty. Furthermore, there is little mention in existing literature of nonlinear whirl flutter studies being conducted. In the design of larger tiltrotor aircraft this shortcoming could be a significant liability [1].

Figure 1: ERICA tiltrotor concept [2]

Due to the unique flight envelope afforded to them through the marriage of VTOL capabilities with fixed wing range and speed, tiltrotors are also an attractive configuration for use in military roles. One of the current specific developmental aims for the tiltrotor configuration is that of maximising cruise speed, and this is where the problem of whirl flutter is encountered.

A rotor or propeller mounted in a wing nacelle may be susceptible to whirl flutter, and the motion itself involves the hub whirling in a circle around its nominal position. Aerodynamic forces acting on the blades and gyroscopic effects acting on the rotor as a whole couple with wing structural modes to produce this unstable vibration, which can damage or even destroy the aircraft structure [3]. With their large and flexible blades, tiltrotors are particularly susceptible to whirl flutter, and it generally limits their maximum cruise speed [4].

The current literature has investigated methods of improving stability margins by alterations to existing rotor designs [5], and studied the impact of effects such as control system stiffness [1]. However, in almost all cases, these studies restricted the modelling of the structural stiffness to linear approximations, which is contingent on the assumption of small deformations. Various kinds of nonlinearity have been shown to have a non-negligible effect on system behaviour. Masarati et al. [6] showed that nonlinear effects at the blade level can have a knock-on effect on overall system

[1] PhD Student, chris.mair@bristol.ac.uk

[2] Lecturer in Aerospace Engineering, djamel.rezgui@bristol.ac.uk

[3] Senior Lecturer in Aerospace Engineering, brano.titurus@bristol.ac.uk

stability, and Krueger [7] showed that nonlinearities introduced by the influence of the drivetrain, free-play and backlash can create a behavioural discrepancy between rotors in windmill and thrust mode. While the main focus of Krueger's paper is to present a multibody modelling approach of an existing ADYN wind tunnel test, the effects of nonlinearity were investigated through the introduction of nonlinear springs in the computational model. Spring stops were also added to provide hard limits on model deflection and a good agreement with the wind tunnel test data was shown. Nonlinear effects are therefore an important modelling consideration, especially in the development of new large tiltrotor aircraft.

Park et al. investigated whirl flutter with a nonlinear structural model [8], though the focus of the paper was an overall design optimization framework as opposed to any impacts on the whirl flutter predictions made by using nonlinear elements in the model. Similarly, investigations by Janetzke et al [9] used nonlinear aerodynamic models adapted from aerofoil data, though the structural aspects of the model did not appear to have benefitted from the same approach.

The application of continuation and bifurcation methods has so far been limited to a small number of helicopter dynamical problems [10], such as flight mechanics, ground resonance and rotor vortex ring state, though their inclusion in rotary wing studies is steadily becoming more prevalent as they are powerful in solving problems such as the identification of instability scenarios of rotor blades [11]. Continuation methods were used in the AW159/Wildcat Release to Service document [12].

In this paper, a basic whirl flutter system is presented in Section 2. This model included linear and subsequently nonlinear stiffness terms in yaw, specifically hardening and softening effects provided by terms proportional to the cube of the displacement. Section 3 describes the stability analysis methods used and these are applied to the linear and nonlinear models as appropriate. The analysis was carried out for a number of cases to study the effects of nonlinearity for a set of selected parameters. The stability results and bifurcation diagrams generated are discussed in Section 4.

2. WHIRL FLUTTER MODEL

A basic model given by Bielawa [13] and originally formulated by Reed [14] was used. In this model, a rotor with moment of inertia about its rotational axis I_x is able to oscillate in pitch θ and yaw ψ about an effective pivot point with moment of inertia I_n. The dynamical contributions of the wing structure are modelled with representative stiffness K and damping C properties in the pitching and yawing directions at the effective pivot point. The system schematic is shown in Figure 2.

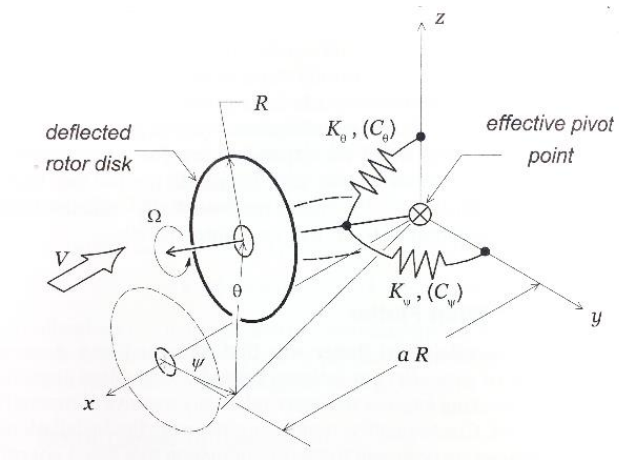

Figure 2: Whirl flutter model schematic adopted from [13]

The original model provided features linear structural stiffness properties and was used as a baseline for comparison with the nonlinear stiffness versions. The equations of motion governing the system, as given by Bielawa, are stated in Equation {1}.

$$\begin{bmatrix} I_n & 0 \\ 0 & I_n \end{bmatrix} \begin{bmatrix} \ddot{\theta} \\ \ddot{\psi} \end{bmatrix} + \begin{bmatrix} C_\theta & -I_x\Omega \\ I_x\Omega & C_\psi \end{bmatrix} \begin{bmatrix} \dot{\theta} \\ \dot{\psi} \end{bmatrix} + \begin{bmatrix} K_\theta & 0 \\ 0 & K_\psi \end{bmatrix} \begin{bmatrix} \theta \\ \psi \end{bmatrix} = \begin{bmatrix} M_\theta \\ M_\psi \end{bmatrix} \quad \{1\}$$

M_θ and M_ψ are aerodynamic moments in pitch and yaw, respectively, and are defined in Equations {2} and {3}. They were derived in the manner employed in Ribner's [15] work on forces and moments generated by propellers experiencing yaw and yawing rates at their hub. Ribner's derivation is founded upon blade element theory and assumes quasi-steady aerodynamics, an aspect that some investigations, such as that by Kim et al [16], have built upon. A key aspect of Ribner's work that separated it from prior art was the inclusion of induction/inflow effects, "analogous to the downwash associated with a finite wing". It can be seen from the equations that there is coupling only at the stiffness level, i.e. proportional to angular displacement rather than velocity.

$$M_\theta = \frac{N_B}{2} K_a R \left[-(A_3 + a^2 A_1)\frac{\dot{\theta}}{\Omega} - A_2'\psi + aA_1'\theta \right] \quad \{2\}$$

$$M_\psi = \frac{N_B}{2} K_a R \left[-(A_3 + a^2 A_1)\frac{\dot{\psi}}{\Omega} + A_2'\theta + aA_1'\psi \right] \quad \{3\}$$

Where: $$K_a = \frac{1}{2}\rho c_{l_\alpha} R^4 \Omega^2$$

K_a is a consolidation of terms for more concise presentation. The A_i terms are aerodynamic integrals that arise from integrating the force expressions along each blade and summing the contributions from each, and can be obtained from [13].

For the nonlinear modelling, the original linear expression for the structural yaw stiffness (i.e. $K_\psi\psi$) was replaced with a polynomial of the form given in Equation {4}, where 'nl' denotes 'nonlinear'. The influence of each term is controlled via dedicated coefficients. The pitch degree of freedom in the original formulation is modelled in exactly the same way, and as such could instead have been selected for nonlinear adaption without any impact on the form of the results.

$$K_{\psi_{nl}}(\psi)\psi = K_1\psi + K_2\psi^3 = (K_1 + K_2\psi^2)\psi \quad \{4\}$$

The nonlinear stiffness expression can provide softening behaviours by using negative values of K_2, and hardening behaviours by using positive values of K_2. Hereafter, the system employing the original linear yaw stiffness expression is referred to as the "linear system", and the systems employing the nonlinear stiffness expressions the "softening system" or "hardening system" as appropriate. The overall shape of these profiles compared to the original linear model is demonstrated in Figure 3.

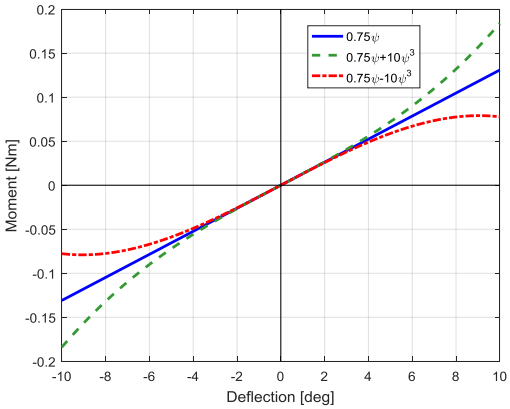

Figure 3: Example nonlinear stiffness profiles

The model equations were written in state-space form, as shown in {5} and {6}.

$$\dot{\mathbf{X}} = f(\mathbf{X}, p), \quad \mathbf{X} \in \mathbb{R}^4, \quad p \in \mathbb{R}^n \quad \{5\}$$

And:

$$\mathbf{X} = \begin{bmatrix} \theta \\ \psi \\ \dot{\theta} \\ \dot{\psi} \end{bmatrix} \quad \{6\}$$

Where **X** is the state vector and p is a vector of parameters. The model was implemented in MATLAB 2016a [17] using the state vector given in {6} and time simulations were generated using the ode45 solver. The parameter values used throughout the investigation were retained where possible from Reed, and are listed in Table 1. Where ranges of parameters were used, the midpoint value was taken for this parameter set. Although these parameters do not represent an actual tiltrotor model, the qualitative results achieved from the following analyses will be applicable to full size tiltrotor aircraft.

Rotor radius	R	0.152 m
Rotor angular velocity	Ω	40 rads^{-1}
Freestream velocity	V	6.7 ms^{-1}
Rotor radius-pivot length ratio	a	0.25
Rotor moment of inertia	I_x	0.000103 kgm^2
Nacelle moment of inertia	I_n	0.000178 kgm^2
Structural pitch damping	C_θ	0.001 Nmsrad^{-1}
Structural pitch stiffness	K_θ	0.4 Nmrad^{-1}
Structural yaw damping	C_ψ	0.001 Nmsrad^{-1}
Structural yaw stiffness	K_ψ	0.4 Nmrad^{-1}
Number of blades	N_B	4
Blade chord	c	0.026 m
Blade lift slope	$c_{l,\alpha}$	2π rad^{-1}

Table 1: Datum parameter values used in MATLAB model.

3. STABILITY ANALYSIS METHODS

Initially, eigenvalue analysis was used to assess the stability of the linear system. This standard method places the equations of motion of the system in

state-space form in order to obtain the Jacobian matrix ***J***, defined as:

$$\dot{\mathbf{X}} = \mathbf{J}\mathbf{X} \qquad \{7\}$$

Where ***X***, the state vector, is defined as in Equation {6}. If the various terms in the aerodynamic moment expressions (Equations {2} and {3}) are brought over to the left-hand side of the equation and incorporated into the relevant matrices, the equations of motion assume the following form:

$$\mathbf{M}\ddot{\mathbf{X}} + \mathbf{C}\dot{\mathbf{X}} + \mathbf{K}\mathbf{X} = \mathbf{0} \qquad \{8\}$$

The Jacobian matrix for this system is therefore:

$$\mathbf{J} = \begin{bmatrix} \mathbf{0} & \mathbf{I} \\ -\mathbf{M}^{-1}\mathbf{K} & -\mathbf{M}^{-1}\mathbf{C} \end{bmatrix} \qquad \{9\}$$

Where ***0*** and ***I*** are 2x2 zero and identity matrices, respectively. The eigenvalues of the Jacobian matrix contain information about the decay rate (i.e. stability) and frequency of the system's vibrational modes, and the corresponding right eigenvectors contain the mode shapes. Scripts for eigenvalue analysis were written in MATLAB so that a direct interface with the model was possible.

For nonlinear systems, numerical continuation and bifurcation theory are used. Continuation calculates the steady-state solutions of a dynamical system as one of its parameters, called the continuation parameter, is varied [11]. The computed solutions construct a number of branches that can be either stable or unstable. To determine their stability, either an eigenvalue or Floquet analysis is carried out at each computed solution point, depending on the nature of the solution. For behaviours considered to be in equilibrium (fixed points), an eigenvalue analysis can be used - requiring local linearization in the case of a nonlinear system - whereas periodic behaviours (limit cycles) require Floquet theory to determine the stability [18].

A bifurcation is a qualitative change in the system behaviour as a parameter is varied. In other words, when the stability of a system is changed or lost, the system bifurcates. The points at which these stability changes happen are called bifurcation points. When the system is nonlinear, new solution branches may emerge from the bifurcation points, leading to the presence of multiple solutions for a given set of system parameters. The identification of these different solution branches helps to uncover the global dynamics of the system. Of particular interest are instances where stability is dependent on the magnitude of a perturbation.

These methods were employed according to the version of the system in question. Bifurcation diagrams were produced using the Dynamical Systems Toolbox for MATLAB by Coetzee [19], which uses an implementation of AUTO-07P [20]. Time simulations were also used in both cases to corroborate the predictions of the stability methods.

4. RESULTS AND DISCUSSION

4.1. Linear stability

Using eigenvalue analysis as described in Section 3 allows the stability of a linear system to be quantified in terms of margin, and the cause of any instability encountered to be recognized through the location of the eigenvalues on the complex plane. The damping ratio and frequency of the linear system's modes are shown in Figure 4 as the freestream velocity V is swept across a range of values.

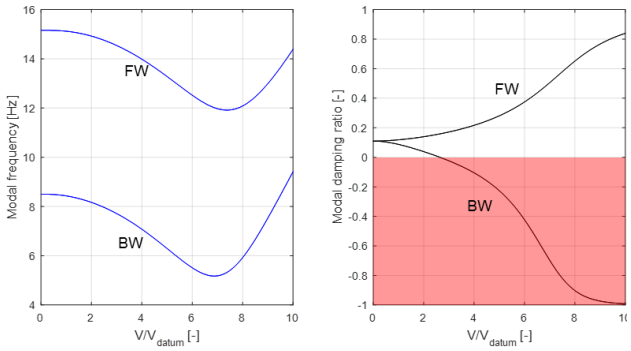

Figure 4: Example frequency (left) and modal damping (right) plots for a sweep in freestream velocity in the linear system, shaded area is unstable. FW denotes the Forward Whirl mode while BW denotes the Backward Whirl mode. Parameters used are presented in Table 1.

The concept of a stability boundary diagram between two parameters can be useful for understanding a system's sensitivity to changes in various parameters, particularly parameters that are readily controllable in the design phase of a practical system, such as a tiltrotor aircraft. Such a diagram can be produced from a grid of the

combinations of different values for each parameter. The Jacobean matrix is calculated at each point, and a surface is overlaid where the level is determined by the maximum real component of the Jacobian's eigenvalues at each point. As the sign of an eigenvalue determines the stability of the corresponding mode – positive being unstable – and only one unstable eigenvalue is required for overall system instability, a horizontal plane cut of this surface at the level 0 will produce a contour that denotes the boundary between the stable and unstable regions of the grid.

One such stability boundary that uses parameters that are controllable in the design phase is that between two structural properties: yaw stiffness K_ψ and pitch stiffness K_θ, shown in Figure 5. To demonstrate the respective impacts of variations in some of the other physical system parameters, the same stability boundary is plotted for a number of such changes. The datum case, using the parameter values given in Table 1, is similar to that achieved by Reed.

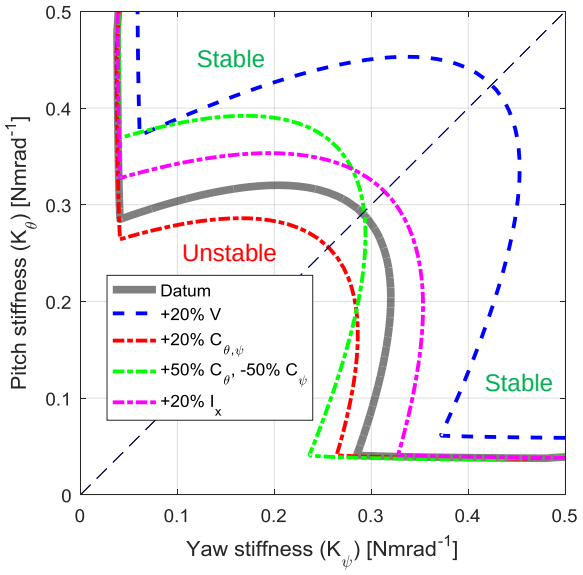

Figure 5: Stability boundary for the linear system in the pitch stiffness and yaw stiffness plane

4.2. Bifurcation analysis

Figure 5 can also be generated by continuation methods, as the system has an equilibrium at $\boldsymbol{X}$ = *[0; 0; 0; 0]* that can be used as a starting solution, and generating the stability boundary this way in fact affords deeper insight than the contour cut method. Key bifurcation types that are relevant to understanding the behaviour of a rotor-nacelle system, particularly when the nonlinear stiffness profiles are introduced, are Hopf bifurcations and branch points. At a Hopf bifurcation, the stability of a fixed point (i.e. an equilibrium) changes, and a periodic solution arises, caused by a pair of complex conjugate eigenvalues crossing the complex plane imaginary axis. At a branch point, the solution changes stability, caused by a single eigenvalue crossing over the complex plane imaginary axis. Because the branch points in this system are of the pitchfork type, two equilibrium branches emanate from the bifurcation point. For more information on the subject, the reader is referred to [21].

Choosing K_θ=0.3 so that a continuation in K_ψ will intersect the regions of interest in the contour-based stability boundary above, the bifurcation diagrams shown in Figure 6 are obtained. In these diagrams, fixed point solutions are plotted, with solid green denoting stability and dashed magenta denoting instability.

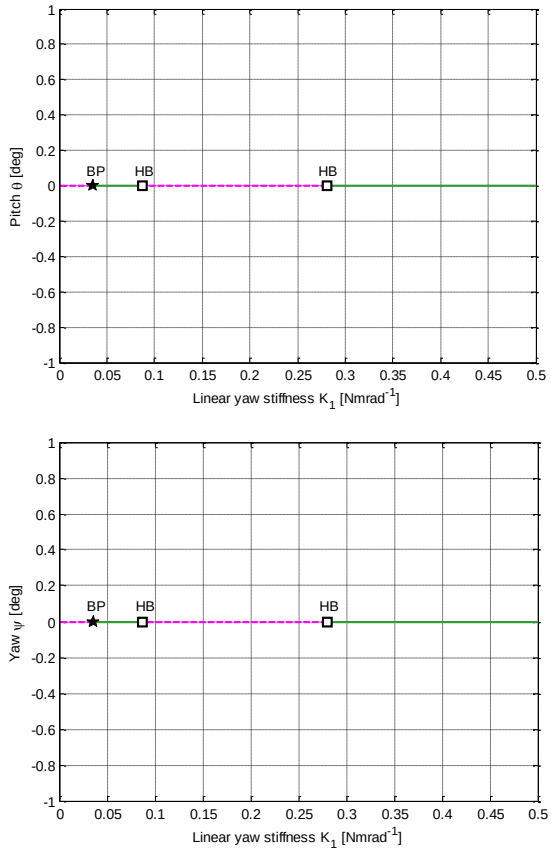

Figure 6: Bifurcation diagram for K_θ*=0.3, for pitch* θ *(top) and yaw* ψ *(bottom) with* K_ψ *as the continuation parameter*

Note the Hopf bifurcation at K_ψ=0.28 (square icon) and the branch point at K_ψ=0.03 (star icon). The bifurcations are visible at the same points in the projections of θ and ψ. The same bifurcation diagram shown in Figure 6 can be generated for different values of K_θ. Alternatively, a two-parameter continuation in K_θ and K_ψ can be performed on the Hopf bifurcation and the branch point to trace their loci in the K_θ-K_ψ plane, and this method is employed here. Plotting these continuations, shown in Figure 7, reconstructs the stability boundary obtained in Figure 5. Now however, the significance of each part of the boundary is known, as well as the path of each segment once inside the unstable region.

As the extent of the curved region in the bottom left corner of the diagram is defined by the location of the Hopf bifurcation for a given combination of K_θ and K_ψ *values*, all points that lie within it have periodic solutions in θ (and in fact all the state variables) – and these motions are the whirl flutter that this paper concerns.

Similarly, the strips that are adjacent to the axes are defined by the branch point, and in terms of physical behaviour, points that lie within these regions are subject to static divergence, where the nacelle is pushed to the side by the aerodynamic forces and moments generated by the rotor. A number of cases of various values of K_θ are selected for further inspection and have been indicated on the graph.

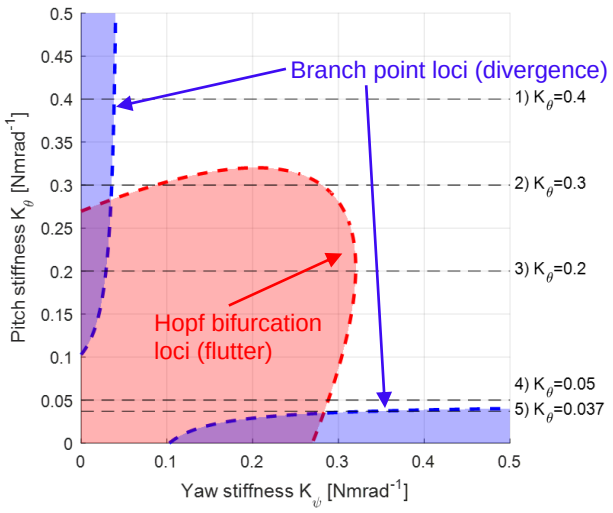

Figure 7: Stability boundary generated by two-parameter continuation. All shaded areas are unstable

As the Hopf and branch point are both on the equilibrium branch, which lies at zero displacement, the positions of the bifurcations do not change with the addition of any nonlinear stiffness terms. However, the dynamic behaviour outside the equilibrium branch calculated in Figure 6 (hereafter referred to as the 'main branch') is affected by nonlinear terms.

Examining cubic hardening first, full bifurcation diagrams for the five cases indicated in Figure 7 were generated by using nonlinear yaw stiffness profiles with a K_2 value of 10, shown in Figure 10. Note that the continuation parameter is now K_1 rather than K_ψ. Initially, case 2 is considered and a more complete diagram is presented in Figure 8. The figure shows complex behaviour manifested in stable and unstable limit cycles and secondary equilibrium branches. While the limit cycle branches illustrate the behaviour of the rotor-nacelle system post whirl flutter, the secondary branches emanating from the branch point bifurcation quantify the static divergence in pitch and yaw according to the value of K_ψ. It is typical in bifurcation analysis to extend the continuation outside the physical range to search for any bifurcations which result in secondary branches extending back to the physical parameter range.

While bifurcation analysis is able to illuminate complex behaviours of a system, the best approach is to supplement continuation with time simulations at points of interest for a fuller understanding. Time histories are shown in Figure 8 for a number of values of K_1, with different initial conditions to demonstrate the stability of limit cycles by showing convergence or divergence as relevant from both sides. From left to right, the areas of interest that are selected for time simulation are the stable static divergence branch (demonstrating convergence on approximately 1.8°), the stable flutter on the static divergence branch (demonstrating convergence on a limit cycle centred at approximately 1.2°), unstable flutter on the main branch (demonstrating divergence from a limit cycle with amplitude of approximately 2° and convergence on a limit cycle with amplitude of approximately 6°) and stable flutter on the main branch (demonstrating convergence on a limit cycle with amplitude of approximately 6.3°).

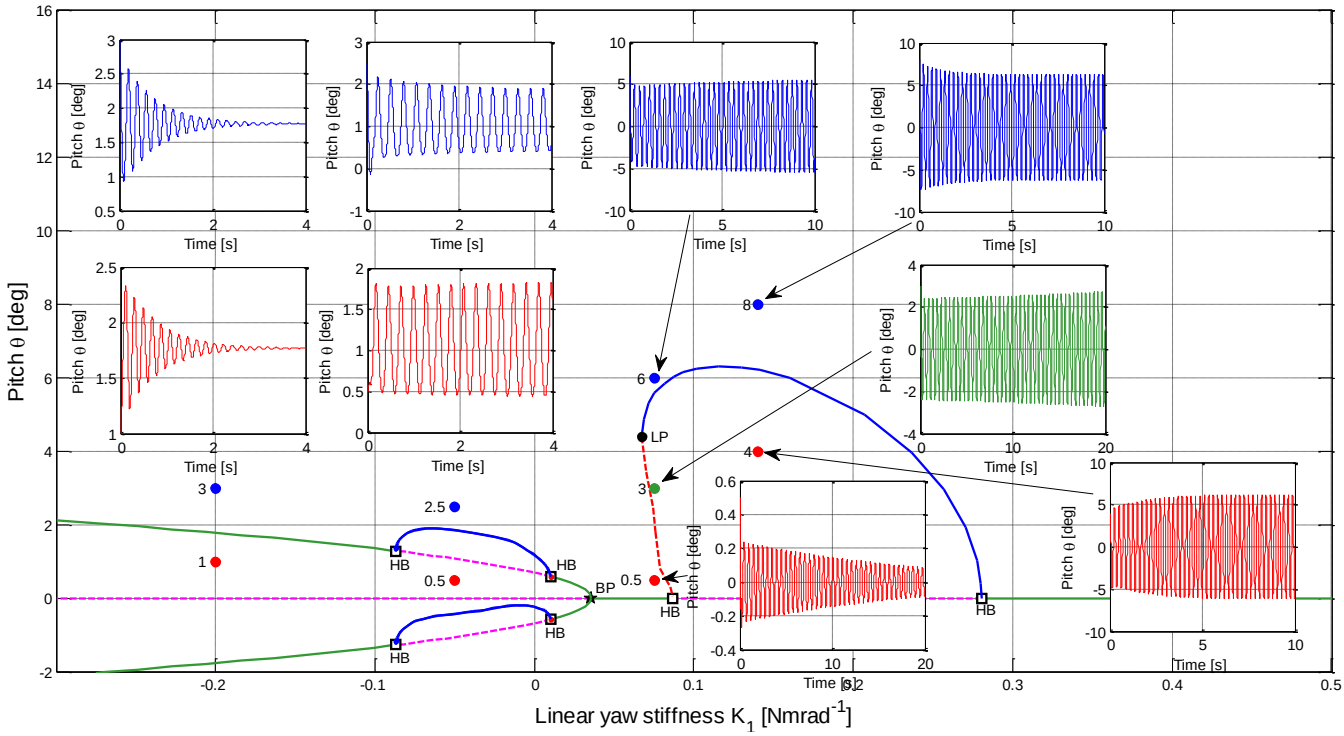

Figure 8: Bifurcation diagram for case 2 (K_θ=0.3) with K_1 as the continuation parameter, complemented with time simulations for a selection of K_1 values

These results are similar to those achieved by Krueger in [7], a study that specifically focuses on whirl flutter in tiltrotors with attention to detail on sources of nonlinearity in the model, as discussed in Section 1. The study simulated a simplified half model of a tiltrotor wing, and studied the effects of parameter changes and nonlinearities on the calculation of the aero-elastic stability boundary. Figure 9 shows comparison of simulation data with wind tunnel data obtained in the European ADYN project, where spring stops have been introduced to limit the motion of the nacelle.

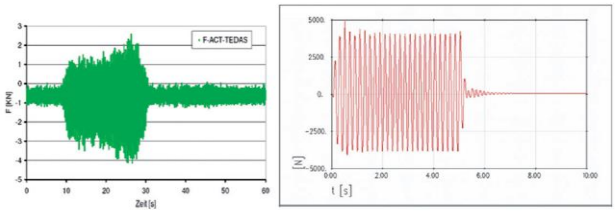

Figure 9: Wind tunnel and simulation data comparison figure from Krueger [7]

While Reed's original model was intended to be representative of proprotors as a whole, it has been shown to also be an appropriate analogue of a tiltrotor's rotor-nacelle system.

4.3. Effects of cubic hardening

Considering each diagram from right to left, i.e. for descending K_1: case 1 (K_θ=0.4) shows divergence only (Figure 10a), case 2 (K_θ=0.3) shows a separate region of flutter only followed by divergence (Figure 10b), case 3 (K_θ=0.2) shows flutter to which divergence is eventually added (Figure 10c), case 4 (K_θ=0.05) shows flutter only (Figure 10d), and case 5 (K_θ=0.037) shows a separate region of divergence followed by flutter (Figure 10e).

For periodic solutions, solid blue denotes the peak amplitude of stable limit cycles, and dashed red denotes the peak amplitude of unstable limit cycles. Only the projection in pitch θ is shown here, though projections in any of the other state variables could also be plotted. Limit points are denoted by 'LP' and reflect a change in stability of a solution branch which folds back at the bifurcation point.

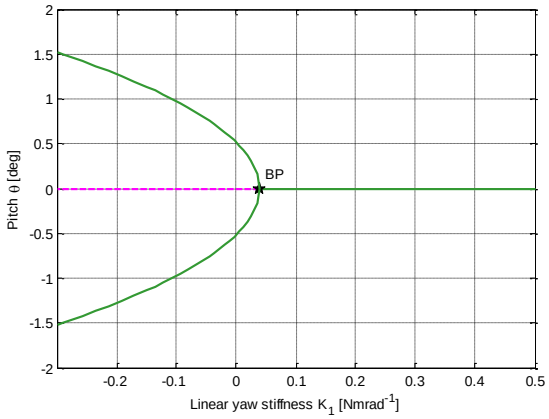

Figure 10a: Bifurcation diagram for case 1 (K_θ=0.4)

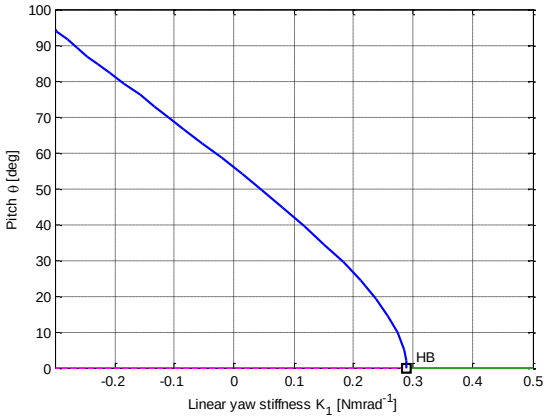

Figure 10d: Bifurcation diagram for case 4 (K_θ=0.05)

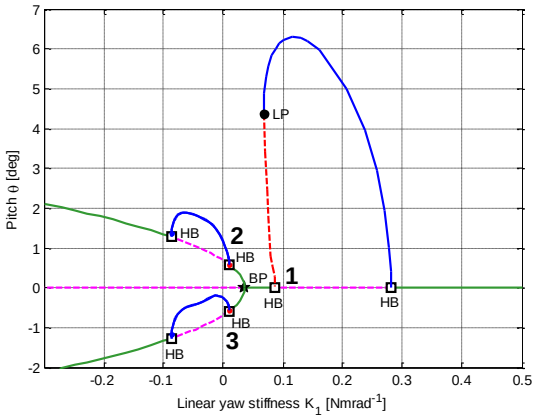

Figure 10b: Bifurcation diagram for case 2 (K_θ=0.3)

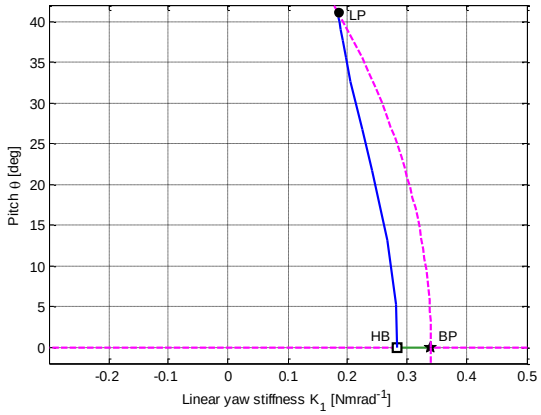

Figure 10e: Bifurcation diagram for case 5 (K_θ=0.037)

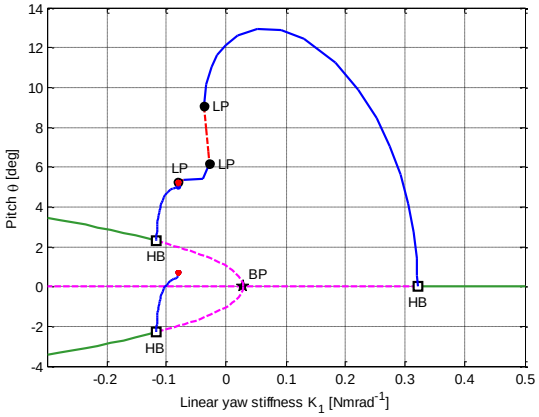

Figure 10c: Bifurcation diagram for case 3 (K_θ=0.2)

Each of the diagrams can be cross-referenced with Figure 7 and the datum case on Figure 5 to confirm that the bifurcations present correspond to the extent of the unstable regions at the relevant value of K_θ. As the value of pitch stiffness is gradually decreased, the amplitude of the limit cycles increases to quite an extent.

Interesting to note is the complex interaction in case 3 (Figure 10a) that occurs between the limit cycles that have formed in case 2 (Figure 10b). While Hopf bifurcation 1 is visible in Figure 7 as it is on the main branch, Hopf bifurcations 2 and 3 are not as they exist on the static divergence secondary branches, and for negative K_ψ/K_1. Between cases 2 and 3, the limit cycle emanating from Hopf bifurcation 1 and the limit cycles emanating from Hopf bifurcations 2 and 3 all increase in both amplitude and their inner-reaching extent, moving toward each other with decreasing K_θ. In case 3, these limit cycles have

collided and a branch point of the limit cycle may therefore be expected at the value of K_ψ at which the peak amplitudes of the divergence-originating limit cycles first make contact with each other.

4.4. Effects of varying K_2

In the above cases, a value of cubic stiffness coefficient K_2 was selected rather arbitrarily in order to effect nonlinear stiffness behaviour. It would therefore be prudent also to understand the effect of the value of K_2. Bifurcation diagrams with K_θ set to 0.3 (as per case 2) for increased and decreased values of K_2 are shown in Figure 11 and Figure 12. As is evident from the plots, increasing K_2 decreases both the amplitude of the flutter and the static divergence for a given value of K_1, due to increasing K_2 making the structure stiffer.

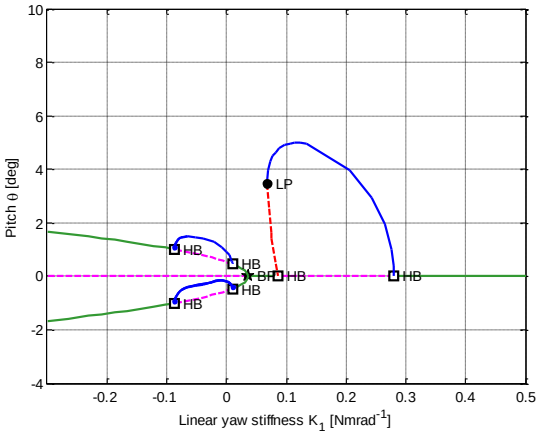

Figure 11: Bifurcation diagram for K_θ*=0.3,* K_2*=16,* K_1 *as continuation parameter*

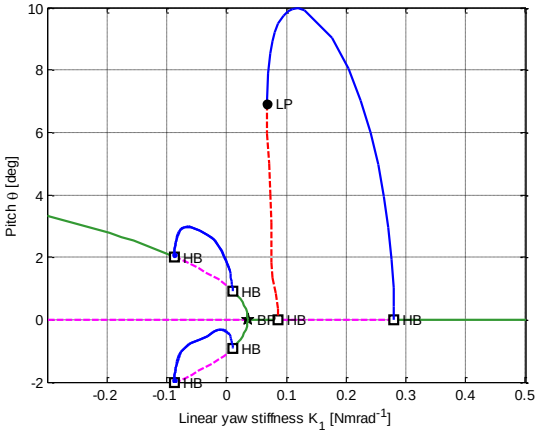

Figure 12: Bifurcation diagram for K_θ*=0.3,* K_2*=4,* K_1 *as continuation parameter*

It is important to note that the family of limit cycle solutions for the main branch Hopf bifurcation always leans over the closing Hopf bifurcation 3, and as a result a portion of the loop connecting to this bifurcation is unstable. It is not possible to remove this unstable region by increasing K_2.

Furthermore, the effects of changing K_2 could also be explored for the other cases shown in Figure 7, though this was deemed outside the scope of this paper.

4.5. Effects of cubic softening

Taking case 2 as an example, the bifurcation diagram using a softening stiffness profile (K_2=-10) was generated and is shown in Figure 13. Time simulations for selected points are shown in subplots. The bifurcations on the main branch still occur in the same left-to-right order as in Figure 10b, as nonlinear stiffness terms do not affect their location, however both the static divergence and flutter behaviours are reversed left-to-right. The static divergence branches, though unstable, overhang the stable portion of the main branch, to the right of the Hopf bifurcation near K_1=0.3. While an unstable flutter solution emanates from this Hopf bifurcation, there is a stable branch with larger amplitude, and both overhang the stable portion of the main branch as far as the limit point at approximately K_1=0.42.

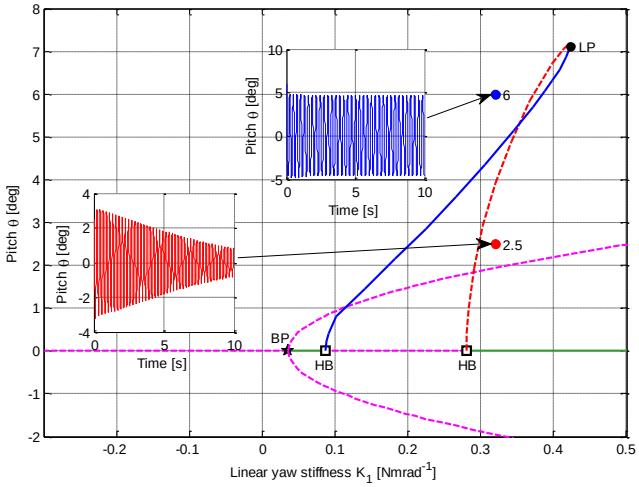

Figure 13: Bifurcation diagram for K_θ*=0.3,* K_2*= -10,* K_1 *as continuation parameter, complemented with time simulations for a selection of initial conditions*

A rotor nacelle mounted on an aircraft is subject to perturbations, either from manoeuvring or gusts. A perturbation of the rotor-nacelle may ultimately bring it sufficiently close to either of these solution branches to experience behaviour of either type. The time simulations show that for K_1=0.32, a point on the stable portion of the main branch, flutter with a slow decay rate is achievable given a pitch perturbation of 2.5°, and stable flutter develops almost immediately with of a perturbation of 6°.

The linear stability analysis has therefore failed to predict the above result. The flutter boundary predicted by this method is the location of the Hopf bifurcation near K_1=0.3, though both flutter and static divergence behaviours are shown to exist for values of K_1 that lie within the stable region.

5. CONCLUSIONS

This paper has demonstrated the use of a basic rotor-nacelle system model for dynamic analysis of whirl flutter behaviours. Both linear and nonlinear stiffness profiles were used for the yaw degree of freedom through addition of a cubic stiffening term. The cubic stiffening behaviours used were softening and hardening. Stability analysis methods were described and employed for linear and nonlinear models. Bifurcation diagrams were generated for a number of hardening cases, and a softening case was shown where whirl flutter was possible in a region where linear analysis would have predicted stability. Where whirl flutter does not cause the loss of an aircraft, oscillations induced by whirl flutter mechanisms present a fatigue hazard to aircraft nacelle mounts.

In the light of these observations, it is advisable to generate revised nonlinear stability boundaries based on the overhang of dynamic behaviours over stable equilibrium branches. Given the likely proliferation of continuation methods and bifurcation analysis in aircraft certification, proper characterisation of aircraft materials and sub-systems is therefore absolutely key, and these stiffness profiles should be used in full nonlinear models for any dynamic analysis conducted. Where analytical functions cannot be fit to material or sub-system stiffness profiles, a table-based approach could be used.

6. ACKNOWLEDGMENTS

The authors would like to kindly thank The UK Engineering and Physical Research Council (EPSRC) for funding this research project.

7. REFERENCES

[1] Acree C. W., Johnson W., *Aeroelastic Stability of the LCTR2 Civil Tiltrotor*, National Aeronautics and Space Administration Moffett Field CA Ames Research Center, 2008

[2] http://www.ltas-aea.ulg.ac.be/cms/uploads-/nicetrip.html. Accessed July 2017

[3] Braniff Airways Flight 542 Accident Report, Civil Aeronautics Board Report SA-346, 1961.

[4] Kunz D. L., *Analysis of Proprotor Whirl Flutter: Review and Update*, Journal of aircraft Vol. 42.1, pp. 172-178, 2005

[5] Acree C. W., Peyran R. J., Johnson W., *Rotor Design Options for Improving Tiltrotor Whirl-Flutter Stability Margins*, Journal of the American Helicopter Society Vol. 46.2, pp. 87-95, 2001

[6] Masarati P., Piatak D. J., Quaranta G., *Soft-inplane tiltrotor aeromechanics investigation using two comprehensive multibody solvers*, Journal of the American Helicopter Society Vol. 53.2, pp. 179-192, 2008

[7] Krueger W. R., *Multibody analysis of whirl flutter stability on a tiltrotor wind tunnel model*, Proceedings of the Institution of Mechanical Engineers, Part K: Journal of Multi-body Dynamics Vol. 230.2, pp. 121-133, 2014

[8] Park J. S., Sung N. J., Myeong-Kyu L., Kim J. M., *Design optimization framework for tiltrotor composite wings considering whirl flutter stability*, Composites Part B: Engineering Vol. 41.4, pp. 257-267, 2010

[9] Janetzke D. C., Kaza K. R. V., *Whirl flutter analysis of a horizontal-axis wind turbine with a two-bladed teetering rotor*, Solar Energy Vol. 31.2, pp. 173-182, 1983

[10] Rezgui D., Lowenberg M. H., *On the nonlinear dynamics of a rotor in autorotation: a combined experimental and numerical approach*, Phil. Trans. R. Soc. A 373.2051 20140411, 2015

[11] Rezgui D., Lowenberg M. H., Jones M., Monteggia C., *Continuation and bifurcation analysis in helicopter aeroelastic stability problems*, J. Guid. Control Dyn. Vol. 37, pp. 889–897, 2014

[12] Jones M., Bernascone A., Masarati P., Quaranta G., Rezgui D., *Ongoing developments in the use of continuation-bifurcation methodology at AgustaWestland*, 2014

[13] Bielawa R. L., *Rotary Wing Structural Dynamics and Aeroelasticity*, Second Edition, Washington, DC: American Institute of Aeronautics and Astronautics, p389, 2005

[14] Reed W. H. III, *Propeller-Rotor Whirl Flutter: A State-of-the-Art Review*, Symposium on the Noise and Loading Actions on Helicopters, V/STOL, and Ground Effect Machines, The University of Southampton, England, August 1966

[15] Ribner H. S., Propellers in Yaw, NACA Report 820, 1945

[16] Kim T., Shin S. J., Taehyoun K., *Analysis of tiltrotor whirl flutter in time and frequency domain*, Journal of mechanical science and technology Vol. 23.12, pp. 3281-3291, 2009

[17] MATLAB 2016a, The MathWorks, Inc., Natick, Massachusetts, United States

[18] Kuchment P. A., *Floquet Theory for Partial Differential Equations*, Vol. 60. Birkhäuser, 2012

[19] Coetzee, E., Krauskopf, B., Lowenberg, M., *The dynamical systems toolbox: Integrating AUTO into MATLAB*, 16th US National Congress of Theoretical and Applied Mechanics, 2010

[20] Doedel E. J., Fairgrieve T. F., Sandstede B., *AUTO-07P: Continuation and bifurcation software for ordinary differential equations*, 2007

[21] Kuznetsov Y. A., *Elements of Applied Bifurcation Theory*, Third Edition, Vol. 112. Springer Science & Business Media, 2004